

# Photoionization of fine structure levels of Ne III

Sultana N. Nahar

Department of Astronomy, The Ohio State University, Columbus, OH 43210, USA

## ARTICLE INFO

### Keywords:

Ne III  
Photoionization  
Cross sections of excited levels  
R-Matrix method  
Resonant features 32.10-  
95.30.Ky  
32.80-T

## ABSTRACT

Detailed study on the characteristic features in photoionization of Ne III, ( $h\nu + \text{Ne III} \rightarrow \text{Ne VI} + e$ ) is reported. The calculations were carried out in relativistic Briet–Pauli R-matrix (BPRM) method and close-coupling (CC) approximation. The CC expansion for the wavefunction of Ne III includes 58 fine structure levels of Ne IV from configurations  $2s^2 2p^3$ ,  $2s 2p^4$ ,  $2p^5$ ,  $2s^2 2p^2 3s$ ,  $2s^2 2p^2 3p$ ,  $2s^2 2p^2 3d$ . The photoionization cross section ( $\sigma_{pi}$ ) features exhibit i) presence of prominent resonances in the low energy region near the ionization thresholds of low lying levels, ii) lower energy region of extensive narrow Rydberg resonances and slow decaying background cross section in the high energy region for equivalent electron levels, and iii) presence of strong Seaton resonances due to photo-excitation-of-core (PEC) in the high energy region. The relativistic effects have almost no impact on the  $\sigma_{pi}$  in the high energy regions. However, for a number of low lying levels the coupling of fine structure channels, which is not allowed in LS coupling, introduces high-peak narrow resonances with almost zero background below the excitation threshold of  $2s^2 2p^3(^2D^o)$  level of the residual ion. These will enhance quantities such as electron-ion recombination, opacity at very low temperature. The Seaton resonances due to  $n=3$  PECs in the high energy region, which was not studied before, are more prominent than those for  $n=2$  PECs. For complete modeling of astrophysical and laboratory plasmas, photoionization cross sections are presented for a large number of excited levels, in total 392, with  $n \leq 10$  and  $l \leq 9$ .

## 1. Introduction

Neon lines observed in astrophysical spectra, such as from planetary nebulae (e.g. Rubin et al., 2001; Rubin, 2004; Dance et al., 2013) and galaxies (e.g. Crockett et al., 2006), can be used for the diagnostics of the objects. The temperature and density diagnostics of nebular photoionized plasma can be determined by the observed Ne III lines. These lines are also common in the star-born galaxies (Ho and Keto, 2007) which produces more stars than typical 1–6 per year and the ionizing photons are produced by the young, hot, massive stars. The Ne lines can provide environmental diagnostics of metallicities, stellar populations, star formation rates and histories, and other interstellar medium properties (Dopita et al., 2006). The spectral analysis of the models require photoionization cross sections. Photoionization cross sections of Ne III have been recently measured at the Advanced Light Source (G. Hinojosa, private communication 2017) prompting high accuracy data needed for the benchmarking.

Very limited study has been carried out on the detailed photoionization of Ne III except for the R-matrix calculations by Butler and Zeppen under the Opacity Project (OP) (The Opacity Project Team, 1995, 1996). The data were not published, but are available at the OP database (TOPbase). Compared to the present work, the earlier

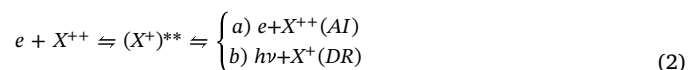
work was carried out nonrelativistic LS coupling approximation and did not study the high energy features due to  $n=3$  excitations in the residual ion. The present results should provide more accurate and complete data for astrophysical and laboratory plasma modeling.

## 2. Theory

Photoionization is a well known process and described in literature (e.g. Pradhan and Nahar, 2011 book AAS). A brief outline is given below for the guidance of the readers. Photoionization occurs directly,



which provides only background cross sections. It can also occur through formation of an intermediate doubly excited autoionization state which leads either to autoionization (AI) where the electron goes to continuum or to dielectronic recombination (DR) where the electron is captured by emission of a photon.



The autoionizing state introduces a resonance in the process. The

E-mail address: [nahar.1@osu.edu](mailto:nahar.1@osu.edu) + 5du.

URL: <http://www.astronomy.ohio-state.edu/~nahar>.

<https://doi.org/10.1016/j.newast.2018.09.011>

Received 29 June 2018; Received in revised form 21 September 2018; Accepted 24 September 2018

Available online 25 September 2018

1384-1076/© 2018 Published by Elsevier B.V.

autoionizing resonance can be described theoretically by including the excitations of the residual ion in the wave function, as considered in close coupling (CC) approximation here.

The CC approximation describes the atomic system of  $(N+1)$  electrons by a 'target' or the 'core' or the residual ion of  $N$ -electrons interacting with the  $(N+1)$ th electron. The total wave function,  $\Psi_E$ , of the  $(N+1)$  electrons system in a symmetry  $SLJ\pi$  is represented by an expansion as

$$\Psi_E(e + ion) = A \sum_i \chi_i(ion)\theta_i + \sum_j c_j \Phi_j, \quad (3)$$

where the target ion eigenfunction,  $\chi_i$ , is coupled with the  $(N+1)$ th electron function,  $\theta_i$ . The first sum is over the ground and excited residual ion states. The  $(N+1)$ th electron with kinetic energy  $k_i^2$  is in a channel labeled as  $S_i L_i J_i \pi_i k_i^2 \ell_i (SLJ\pi)$ . In the second sum, the  $\Phi_j$ s are bound channel functions of the  $(N+1)$ -electrons system that account for short range correlation and the orthogonality between the continuum and the bound electron orbitals.

The relativistic effects are included through Breit-Pauli approximation (e.g. Hummer et al., 1993; Pradhan and Nahar, 2011) where the Hamiltonian of the  $(N+1)$ -electrons system in Rydberg unit (1/2 of Hartree) is written as

$$H_{N+1}^{BP} = \sum_{i=1}^{N+1} \left\{ -\nabla_i^2 - \frac{2Z}{r_i} + \sum_{j>i}^{N+1} \frac{2}{r_{ij}} \right\} + H_{N+1}^{mass} + H_{N+1}^{Dar} + H_{N+1}^{so} \quad (4)$$

The additional terms are the relativistic one-body correction terms, the mass correction,  $H^{mass} = -\frac{\alpha^2}{4} \sum_i p_i^4$ , Darwin,  $H^{Dar} = \frac{Z\alpha^2}{4} \sum_i \nabla^2(\frac{1}{r_i})$ , and the spin-orbit interaction,  $H^{so} = Z\alpha^2 \sum_i \frac{1}{r_i} \mathbf{l}_i \cdot \mathbf{s}_i$ . Under the Iron Project (IP, Hummer et al., 1993) the Breit-Pauli R-matrix (BPRM) method includes these and part of two-body interaction terms, which are without the momentum operators (e.g. Pradhan and Nahar, 2011).

Substitution of the CC wavefunction  $\Psi_E(e + ion)$  in the Schrodinger equation

$$H_{N+1} \Psi_E = E \Psi_E \quad (5)$$

introduces a set of coupled equations that are solved using the R-matrix approach. The details of the R-matrix method in the CC approximation can be found in references (e.g. Burke and Robb, 1975; Seaton, 1987; Berrington et al., 1987; Berrington et al., 1995; Pradhan and Nahar, 2011). In BPRM method, the set of  $SL\pi$  is recoupled for  $J\pi$  levels of  $(e + ion)$  system which is followed by diagonalization of the Hamiltonian. The solution is a continuum wave function,  $\Psi_F$ , for an electron with positive energies ( $E > 0$ ), or a bound state,  $\Psi_B$ , at a negative total energy ( $E \leq 0$ ).

Transition matrix elements for photoionization,  $\langle \Psi_B || \mathbf{D} || \Psi_F \rangle$  where  $\mathbf{D} = \sum_i \mathbf{r}_i$  is the dipole operator and the sum is over the number of electrons, are obtained from the bound  $\Psi_B$  and continuum  $\Psi_F$  wave functions. The transition matrix element gives the generalized line strength  $\mathbf{S}$  as

$$\mathbf{S} = |\langle \Psi_f || \mathbf{D}_L || \Psi_i \rangle|^2 = \left| \left\langle \psi_f \left| \sum_{j=1}^{N+1} r_j \right| \psi_i \right\rangle \right|^2, \quad (6)$$

where  $\Psi_i$  and  $\Psi_f$  are the initial and final state wave functions and photoionization cross section ( $\sigma_{PI}$ ) is obtained as,

$$\sigma_{PI} = \frac{4\pi^2}{3c} \frac{1}{g_i} \omega \mathbf{S}, \quad (7)$$

where  $g_i$  is the statistical weight factor of the bound state and  $\omega$  is the incident photon energy. Radiation damping of the resonances (Zhang et al., 1999) has been included. The complex resonant structures in photoionization result from channel couplings between continuum channels that are open ( $k_i^2 > 0$ ), and ones that are closed ( $k_i^2 < 0$ ), at electron energies  $k_i^2$  corresponding to autoionizing states of the

**Table 1**

Levels and energies ( $E_i$ ) of the residual ion Ne IV included in the wavefunction expansion of Ne III, and comparison with observed values at the compiled table of the NIST.

	Level	$J_i$	$E_i$ (Ry) NIST	$E_i$ (Ry) SS
1	$1s^2 2s^2 2p^3 (^4S^o)$	3/2	0.0	0.
2	$1s^2 2s^2 2p^3 (^2D^o)$	5/2	0.375758	0.4143
3	$1s^2 2s^2 2p^3 (^2D^o)$	3/2	0.37616	0.4139
4	$1s^2 2s^2 2p^3 (^2P^o)$	3/2	0.5690	0.5796
5	$1s^2 2s^2 2p^3 (^2P^o)$	1/2	0.5689	0.5793
6	$1s^2 2s 2p^4 (^4P)$	5/2	1.6755	1.6906
7	$1s^2 2s 2p^4 (^4P)$	3/2	1.6811	1.6961
8	$1s^2 2s 2p^4 (^4P)$	1/2	1.6840	1.6993
9	$1s^2 2s 2p^4 (^2D)$	5/2	2.3153	2.4326
10	$1s^2 2s 2p^4 (^2D)$	3/2	2.3155	2.4325
11	$1s^2 2s 2p^4 (^2S)$	1/2	2.7304	2.8349
12	$1s^2 2s 2p^4 (^2P)$	3/2	2.9163	3.1095
13	$1s^2 2s 2p^4 (^2P)$	1/2	2.9228	3.1162
14	$1s^2 2s^2 2p^2 3s (^4P)$	1/2	4.3622	4.3915
15	$1s^2 2s^2 2p^2 3s (^4P)$	3/2	4.3657	4.3949
16	$1s^2 2s^2 2p^2 3s (^4P)$	5/2	4.3710	4.4006
17	$1s^2 2p^5 (^2P^o)$	3/2	4.4188	4.6890
18	$1s^2 2p^5 (^2P^o)$	1/2	4.4275	4.6986
19	$1s^2 2s^2 2p^2 3s (^2P)$	1/2	4.4516	4.4976
20	$1s^2 2s^2 2p^2 3s (^2P)$	3/2	4.4579	4.5043
21	$1s^2 2s^2 2p^2 3p (^2S^o)$	1/2		4.7018
22	$1s^2 2s^2 2p^2 3s (^2D)$	5/2	4.6628	4.7094
23	$1s^2 2s^2 2p^2 3s (^2D)$	3/2	4.6630	4.7094
24	$1s^2 2s^2 2p^2 3p (^4D^o)$	1/2	4.7478	4.7572
25	$1s^2 2s^2 2p^2 3p (^4D^o)$	3/2	4.7498	4.7592
26	$1s^2 2s^2 2p^2 3p (^4D^o)$	5/2	4.7530	4.7626
27	$1s^2 2s^2 2p^2 3p (^4D^o)$	7/2	4.7573	4.7674
28	$1s^2 2s^2 2p^2 3p (^4P^o)$	1/2	4.7795	4.7965
29	$1s^2 2s^2 2p^2 3p (^4P^o)$	3/2	4.7812	4.7984
30	$1s^2 2s^2 2p^2 3p (^4P^o)$	5/2	4.7844	4.8018
31	$1s^2 2s^2 2p^2 3p (^2D^o)$	3/2	4.8367	4.8643
32	$1s^2 2s^2 2p^2 3p (^2D^o)$	5/2	4.8569	4.8710
33	$1s^2 2s^2 2p^2 3p (^4S^o)$	3/2	4.8569	4.8730
34	$1s^2 2s 2p^3 3s (^6S^o)$	5/2	4.9072	5.0673
35	$1s^2 2s^2 2p^2 3p (^2P^o)$	1/2		4.9367
36	$1s^2 2s^2 2p^2 3p (^2P^o)$	3/2		4.9372
37	$1s^2 2s^2 2p^2 3s (^2S)$	1/2	5.0301	5.1169
38	$1s^2 2s^2 2p^2 3p (^2F^o)$	5/2	5.0602	5.0983
39	$1s^2 2s^2 2p^2 3p (^2F^o)$	7/2	5.0614	5.0997
40	$1s^2 2s^2 2p^2 3p (^2D^o)$	5/2	5.1133	5.1863
41	$1s^2 2s^2 2p^2 3p (^2D^o)$	3/2	5.1143	5.1868
42	$1s^2 2s^2 2p^2 3p (^2P^o)$	1/2		5.2463
43	$1s^2 2s^2 2p^2 3p (^2P^o)$	3/2		5.2495
44	$1s^2 2s^2 2p^2 3d (^2P)$	3/2	5.2511	5.3040
45	$1s^2 2s^2 2p^2 3d (^4F)$	3/2		5.2679
46	$1s^2 2s^2 2p^2 3d (^4F)$	5/2		5.2697
47	$1s^2 2s^2 2p^2 3d (^4F)$	7/2		5.2725
48	$1s^2 2s^2 2p^2 3d (^4F)$	9/2		5.2761
49	$1s^2 2s^2 2p^2 3d (^2P)$	1/2	5.2547	5.3116
50	$1s^2 2s^2 2p^2 3d (^2D)$	3/2	5.2599	5.4149
51	$1s^2 2s^2 2p^2 3d (^2D)$	5/2	5.2599	5.4168
52	$1s^2 2s^2 2p^2 3d (^4P)$	5/2	5.2790	5.3275
53	$1s^2 2s^2 2p^2 3d (^4P)$	3/2	5.2819	5.3300
54	$1s^2 2s^2 2p^2 3d (^4P)$	1/2	5.2830	5.3313
55	$1s^2 2s^2 2p^2 3d (^4D)$	1/2		5.3059
56	$1s^2 2s^2 2p^2 3d (^4D)$	5/2		5.3090
57	$1s^2 2s^2 2p^2 3d (^4D)$	3/2		5.3092
58	$1s^2 2s^2 2p^2 3d (^4D)$	7/2		5.3109

Rydberg series,  $S_i L_i J_i \pi_i \nu \ell$  where  $\nu$  is the effective quantum number, converging to the target thresholds.

### 3. Computation

The BPRM calculation involves number of stages of computations through the package of BPRM codes (Berrington et al., 1987; 1995). R-matrix computations begin at stage 1 using the code named STG1 which takes the wavefunction of the residual ion as the input. The wavefunction of the residual ion Ne IV has been obtained using the analytic

Download English Version:

<https://daneshyari.com/en/article/11029471>

Download Persian Version:

<https://daneshyari.com/article/11029471>

[Daneshyari.com](https://daneshyari.com)